COBEM 2021 26th International Congress of Mechanical Engineering
ABCM Associação Brasileira de Engenharia e Ciências Mecânicas
November 22-26, 2021, Virtual Congress, Brazil

COB-2021-0648
NUMERICAL COMPARATIVE STUDY OF HEAT EXCHANGER COILS

Jonatha Wallace da Silva Araújo[1]
Felipe Pinheiro Maia[1]
Ramon Carneiro[2]
Sandi Itamar Schafer de Souza[1]

[1]Federal University of Rio Grande do Norte, Department of Mechanical Engineering, Natal, Postal Code 59072-970, Brazil
jonatha_wallace@hotmail.com, felipepm99@hotmail.com, sandi.souza@ufrn.br

[2]Aeronautics Institute of Technology, Aerospace Science and Technology Graduate Program, São José dos Campos, Postal Code 12228-900, Brazil.ramon_cgd@hotmail.com

Abstract. *One of the most common applications in any industry is the heat exchangers, i.e., devices that use the temperature difference between fluids in flow as a mechanism to promote the thermal energy flux between separated systems. Examples of heat exchanger applications are the evaporation and condensation processes of refrigeration systems, the heating or cooling process of food products, heat regenerative systems and the processing of industrial products. The development of studies aimed at increasing the efficiency of thermal exchange processes has great importance in this economic scenario. According to this, the objective of this paper was to analyze, using Computational Fluid Dynamics (CFD) methods, four different coil geometries for a shell and tube heat exchanger. To this study, the coils selected are a helical geometry, geometry with vertical ducts and horizontal ducts, and a straight duct used as the reference, all with the size delimited by a determined maximum shell volume. The simulations were performed following the RANS method and using the k-ω-SST model to calculate the turbulent flows. Unstructured meshes formed by tetrahedral elements were adopted to the domain's discretization and the necessary wall treatment required by the model was applied. The fluid used to flow into the coils is the water. As a boundary condition for the three geometries was imposed the prescribed coil surface temperature of 25°C and the inlet flow with uniform velocity profile equivalent to Reynolds numbers 3000, 6000, 9000, 12000 and 15000, average temperature of 100°C, and turbulent intensity of 5 %. As a result of these simulations, the general aspects of the flow into the coils, the Nusselt number curves for each case, as a function of the Reynolds number, and the respective pressure drop for the four configurations were obtained. With such data, the best geometry for heat exchange in the determined volume can be identified in terms of thermal efficiency.*

Keywords: *Heat Exchanger, Coil, Thermal Analysis, CFD, RANS.*

1. INTRODUCTION

Heat exchangers are widely used in engineering applications involving heating or cooling systems. Typically, these devices make use of fundamentals of thermal sciences, such as the forced flow of fluids inside tubes and ducts. According to Bergman et al. (2014), the internal flow configuration can represent and model a series of applications, such as the heat transfer process used in chemical processes, environmental control, and energy conversion processes.

Heat exchangers consist of devices that have coils long enough to guarantee the heat transfer conditions necessary for a certain process. Studies that seek to optimize the best geometric arrangements for heat exchangers are quite frequent in the literature.

Among some works available in the literature that present studies related to the thermal exchange mechanism, as well as ways to intensify this phenomenon, can be cited the Vivekanandan *et al*. (2020), which presents a numerical-experimental study in which deflector plates are used inside the shell of a shell-tube heat exchanger in order to promote an increase in the time in contact with the internal helical tube by which the fluid is cooled. Chang *et al*. (2020) presents a numerical study of internal flow inside helical tubes and ducts. In this study, the authors verified an increase in the heat transfer rates by introducing a torsion in the cross-section profile of the pipeline, which caused the effects of secondary flow (swirl) to dominate the heat exchange process. Fouda et al. (2017) developed a numerical study where the heat transfer and performance characteristics of a helical type exchanger were investigated. The numerical results showed the increase of the heat transfer coefficient with the Reynold Number of the flow. This work also investigated the efficiency of the exchanger in terms of the Thermal-hydrodynamic performance index (ε), defined as the ratio between the transferred heat and the obtained pressure drop. A significant enhancement in the efficiency of the system was observed as the diameter of the cross section was increased, due to the reduction in head loss.

Given this scenario, the present work aimed to numerically investigate three configurations of coil arrangement for application in heat exchangers, in order to verify which of the models provides better performance in terms of heat exchange. General aspects of the flow on each model will also be presented.

2. NUMERICAL PROCEDURE

In this paper, four different configurations of coils for a shell and tube heat exchanger were evaluated. Figure 1 presents a conceptual model of such configurations emphasizing, inside the devices, the region to be analyzed. One of these four configurations, the straight tube case (case A), was defined as a comparison parameter. This is reasonable because, despite of the case A area is different from the other cases, the heat transfer is analyzed in this paper using dimensionless parameters that considers the surface area of each coil.

Cases B, C and D were developed to guarantee approximately the same coil length, with the main difference being only the geometric arrangement. The internal diameter of the cross-section (D) used was 20 mm.

In the study in question, the analyzes were performed only in the duct region to simplify the numerical simulations. For the four cases, the same boundary condition was applied to the wall, defined to represent the flow outside the ducts. The condition imposed was the prescribed temperature on the wall.

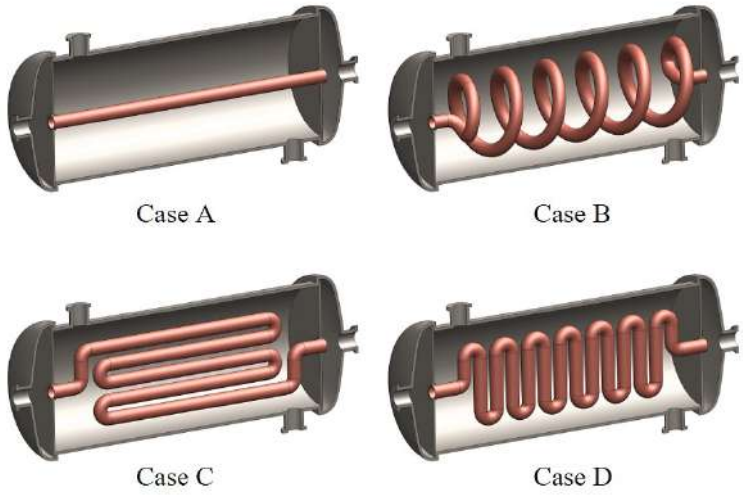

Figure 1. Conceptual representation of the heat exchangers analyzed.

Figure 2 presents the simplified geometric models, with the appropriate impositions for the boundary conditions. As input condition (inlet), was defined the value of the average speed in the cross-section, such as the parameters of the closure model selected ($k - \omega$ SST model).

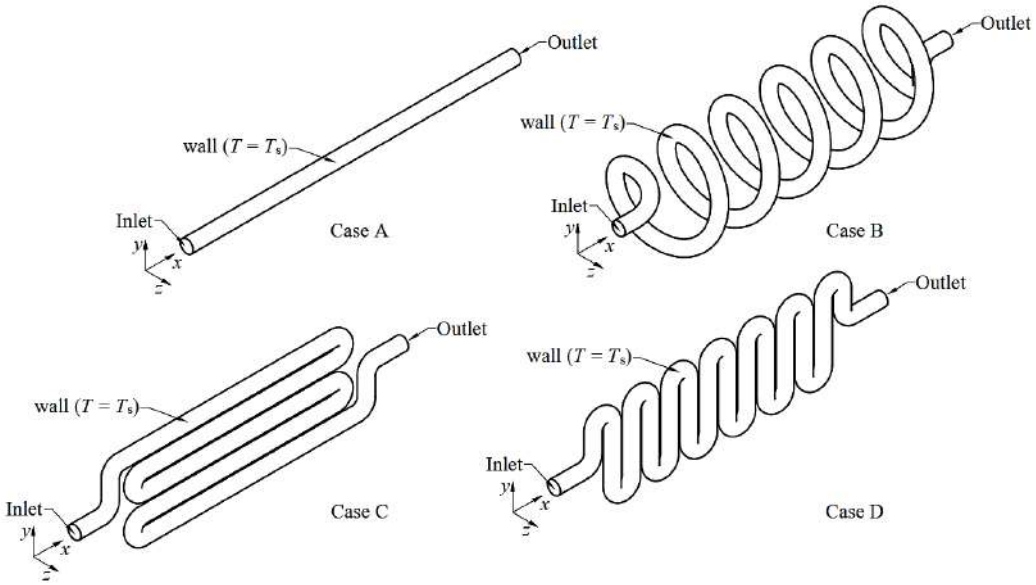

Figure 2. Simplified geometric models.

The velocity imposed at the inlet varied as a function of the Reynolds number (Re). The values of Reynolds number adopted for the analysis were 3000, 6000, 9000, 12000 and 15000. In addition, a turbulence intensity of 5% and a uniform temperature of 100°C were defined at the inlet. At the outlet, atmospheric pressure was admitted. The wall was fixed, in all cases, at a fixed temperature of T_s = 25 ºC.

Figures 3 and 4 show the computational meshes used in the simulations. In cases A, C and D, multizone meshes were used with predominantly hexahedral elements, while in case B a polyhedral mesh was generated. In all cases, there was preferential refining to the wall in order to guarantee that the prismatic layers satisfied the condition of $y^+ < 1$, a necessary condition to establish the correct performance of the closure model adopted. Besides that, this wall condition is essential to ensure the correct capture of velocity and thermal gradients in the region adjacent to the wall.

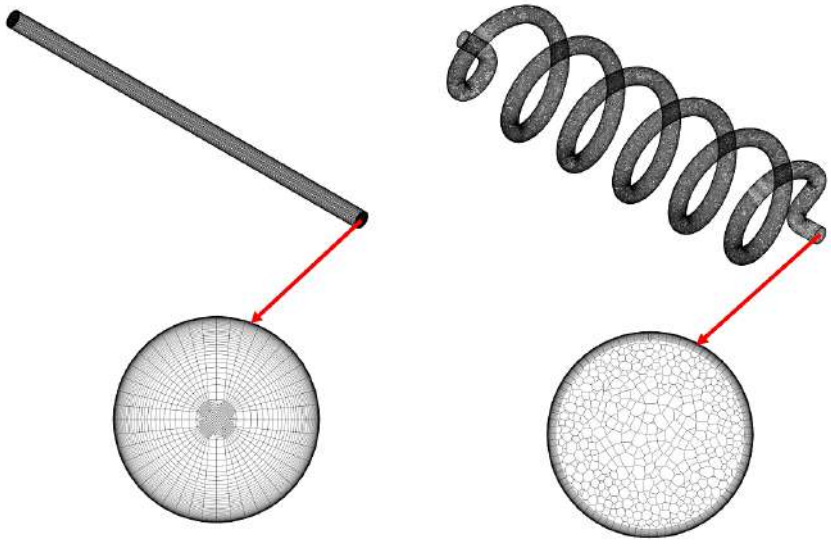

Figure 4. Computational meshes for cases A and B.

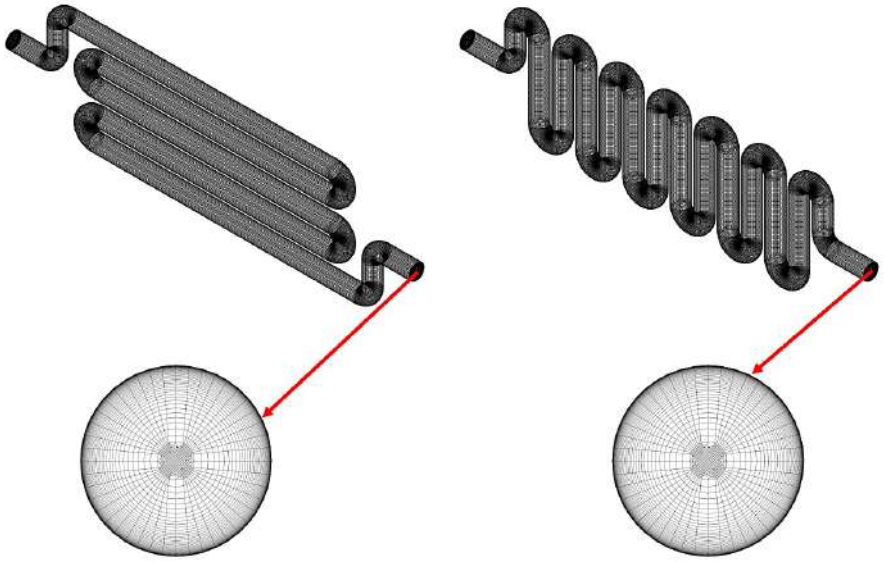

Figure 3. Computational meshes for cases C and D.

RANS (Reynolds Average Navier-Stokes) steady-state simulations were developed, with the FLUENT software as the solver utilized. The governing equations resolved were the average forms of the mass conservation, momentum conservation, and energy conservation equations, as presented by Versteeg and Malalasekera (2007). Such equations are described in Eqs. 1, 2 and 3.

$$\frac{\partial\left(\rho\bar{u}_i\right)}{\partial x_i} = 0 \tag{1}$$

$$\frac{\partial\left(\rho\overline{u}_j\overline{u}_i\right)}{\partial x_j}=-\frac{\partial\overline{p}}{\partial x_j}+\frac{\partial}{\partial x_j}\left[\left(\mu+\mu_t\right)\left(\frac{\partial\overline{u}_i}{\partial x_j}+\frac{\partial\overline{u}_j}{\partial x_i}\right)\right]+\frac{\partial}{\partial x_j}\left[\frac{1}{3}\left(\mu+\mu_t\right)\frac{\partial\overline{u}_i}{\partial x_j}\delta_{ij}\right] \tag{2}$$

$$\frac{\partial\left(\overline{u}_j\overline{T}\right)}{\partial x_j}=\frac{\partial}{\partial x_j}\left[\left(\alpha+\alpha_t\right)\frac{\partial\overline{T}}{\partial x_j}\right]+\phi \tag{3}$$

where ρ is the water density, p is the pressure, T is the temperature, u_i is the flow velocity, μ is the fluid dynamic viscosity, α is the thermal diffusivity, μ_t is the turbulent dynamic viscosity e α_t a is the turbulent thermal diffusivity. The term ϕ (Eq. 4) represents the viscous dissipation function, while the subscripts i and j can assume the values from 1 to 3, representing the spatial coordinates x, y and z, respectively.

$$\phi=-\frac{2}{3}\mu\left(\frac{\partial\overline{u}_j}{\partial x_j}\right)^2+\frac{\mu}{2}\left(\frac{\partial\overline{u}_j}{\partial x_i}+\frac{\partial\overline{u}_i}{\partial x_j}\right)^2 \tag{4}$$

For the turbulence closure model, two more equations are added to the differential equations system. They are the turbulent kinetic energy transport equation (k) and the transport equation for the specific dissipation rate (ω), showed in Eqs. 5 and 6.

$$\frac{\partial\left(\rho k\overline{u}_i\right)}{\partial x_i}=\frac{\partial}{\partial x_j}\left(\Gamma_k\frac{\partial k}{\partial x_j}\right)+G_k-Y_k \tag{5}$$

$$\frac{\partial\left(\rho\omega\overline{u}_i\right)}{\partial x_i}=\frac{\partial}{\partial x_j}\left(\Gamma_\omega\frac{\partial\omega}{\partial x_j}\right)+G_\omega-Y_\omega \tag{6}$$

where G_k is the term of k generation, Y_k is the k dissipation, Γ_k is the k effective diffusivity, G_ω is the term of ω generation, Y_ω is the ω dissipation and Γ_ω the ω effective diffusivity. More details can be founded in Wilcox (2008).

The fluid selected for the analysis is the water with constant properties taken for an average temperature of 62.5 °C. Table 1 summarizes the properties considered in this paper.

Table 1. Water properties at average temperature of 62.5 °C.

Density (kg/m³)	**Specific Heat** (J/kg.K)	**Thermal Conductivity** (Wm.K)	**Dynamic Viscous** (Pa.s)
981.54	4182	0.6	4.3756×10^{-4}

In order to guarantee the independence of the numerical results with the mesh resolution adopted, the Grid Convergence Index (GCI) method was applied closely following Çelik et al. (2008). This method demands the generation of three meshes with different resolutions related to each other by a refinement ratio (r) of about 1.3 or more. The GCI index is calculated from the quantitative comparison of a physical parameter obtained from the meshes simulations. In this paper, the GCI method was applied considering only the helicoidal coil domain, and the analysis parameter selected was the temperature in the outlet of the coil. The meshes generated are presented in Tab. 2, as well as the outlet temperatures registered, and the GCI index calculated between the meshes.

Table 2. Grid Convergence Index analysis.

	Number of cells	Average cell size (mm)	Outlet temperature (K)
Mesh 1	5.49 x 10^6	0.51	321.72
Mesh 2	2.54 x 10^6	0.66	321.15
Mesh 3	1.14 x 10^6	0.86	320.11
GCI index	r_{32} = 1.3064		r_{21} = 1.2928
	0.54%		0.31%

The GCI indexes calculated are less than 1%, what indicates that, for the meshes adopted in this study, the resolution has a minor influence on the heat transfer numerical results obtained. In this way, the resolution of Mesh 2 was adopted for the discretization of all the domains analyzed in this paper.

2.1 Thermal analysis

To calculate the average heat transfer coefficient by convection, an energy balance between the inlet and outlet region of the ducts was used (Eq. 7), as presented by Bergman et al. (2014).

$$\bar{h} = \frac{\dot{m} c_p \left(T_{in} - T_{out}\right)}{A_s \Delta T_{ml}} \tag{7}$$

where ΔT_{ml} represents the logarithmic average temperature of the problem analyzed, defined according to Eq. 8, As is the surface area of each tube and cp is the specific heat at constant pressure.

$$\Delta T_{ml} = \frac{T_{in} - T_{out}}{\ln\left[\left(T_{out} - T_s\right)/\left(T_{in} - T_s\right)\right]} \tag{8}$$

Based on the average convective coefficient, the average Nusselt number for each configuration was obtained using Eq. 9.

$$\overline{Nu} = \frac{\bar{h} D}{k} \tag{9}$$

where k is the water thermal conductivity at 62.5°C and D the internal diameter of the analyzed tubes (20 mm).

In addition, the cost-benefit relation proposed by Fouda *et al*. (2018), namely the thermal-hydrodynamic performance index (ε), was applied to evaluate the relation between the total heat transfer (Q) and the pressure drop (ΔP). This parameter is defined in Eq. 10.

$$\varepsilon = \frac{Q}{\Delta P} \tag{10}$$

Finally, for the quantification of the intensity of the secondary flow (Dean vortices) downstream the pipe knees, the Dean number is calculated as defined in Eq. 11.

$$De = \mathrm{Re}\sqrt{\frac{D}{2R_c}} \tag{11}$$

where Re is the Reynolds number and R_c is the curvature radius, equal to 30 mm in all the cases considered in this paper.

3. RESULTS AND DISCUSSIONS

Based on the procedure described above, the flow along the coils was analyzed. Figure 4 presents the behavior of the streamlines for the four geometries analyzed in this paper. As the phenomenon observed in the flow does not change with the change of the Reynolds number, only the results for Reynolds number 3000 and 15000 are presented.

Figure 4. Streamlines along the heat exchanger coils for Reynolds numbers 3000 and 15000. Some cross-sections of interest are indicated for further analysis.

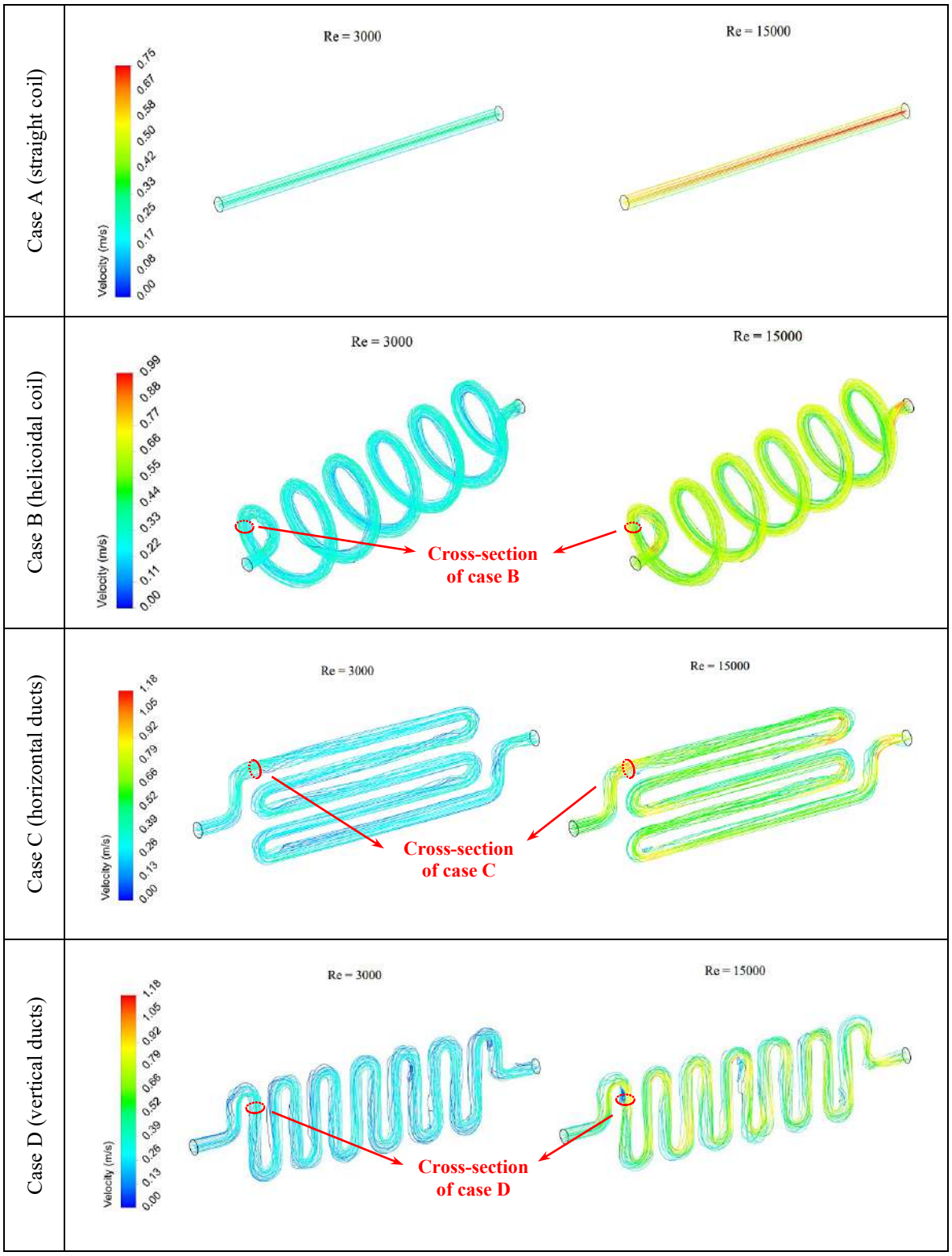

As can be seen in Figure 4, the more abrupt changes in the flow direction, the more disturbed is the flow. The streamlines in case A had practically no three-dimensional effects, while case D had multiple recirculation zones, especially after each abrupt change in the flow direction occurred in the pipe knees. Cases B and C also showed detachment and recirculation zones but in smaller intensity. Detailed views of the flows in cross-sections of each coil are presented in Fig. 5, 6 and 7 for cases B, C and D, respectively. The cross-section of case A is not shown because does not presents three-dimensional effects. In all cases, the cross-section was taken after the first change in the flow direction, such as the duct inclinations or duct knees, according to the pointed out in the Fig. 4.

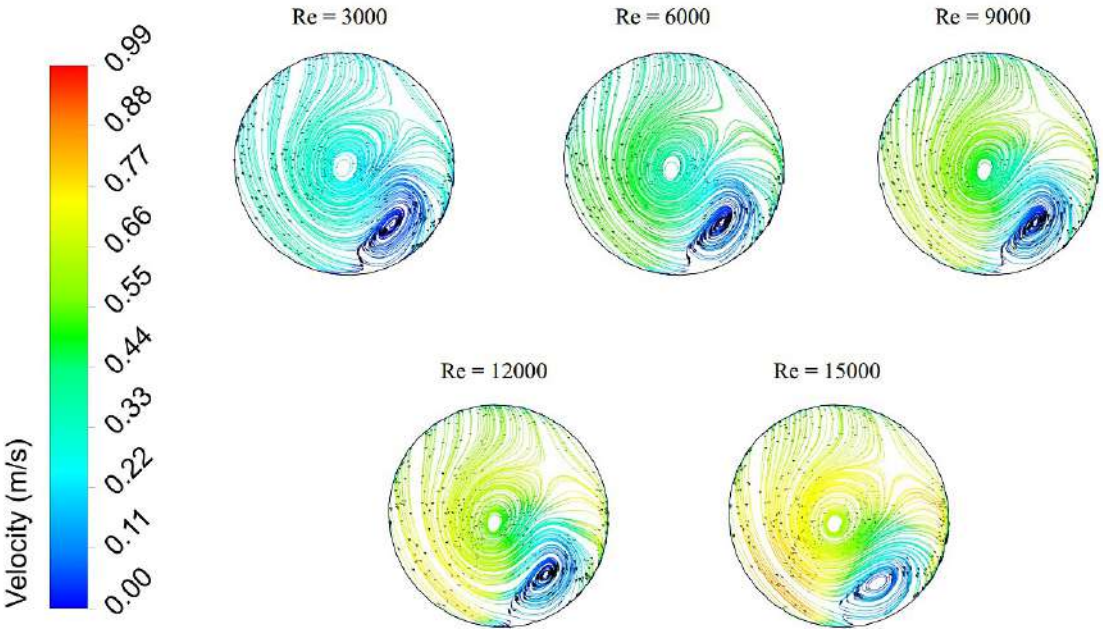

Figure 5. Streamlines at the cross-section of case B.

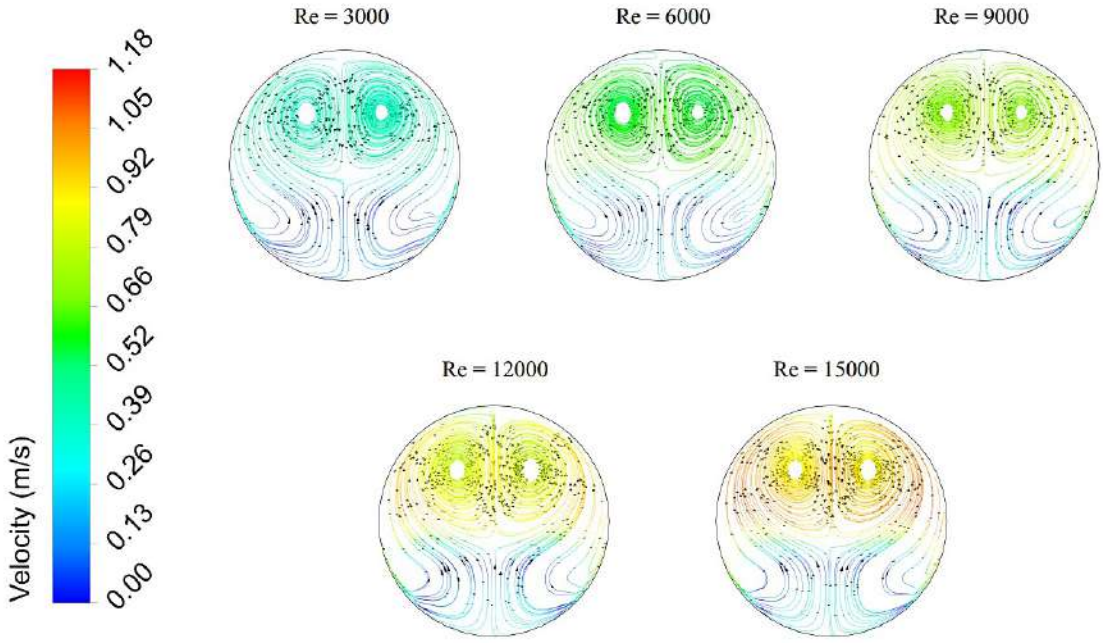

Figure 6. Streamlines at the cross-section of case C.

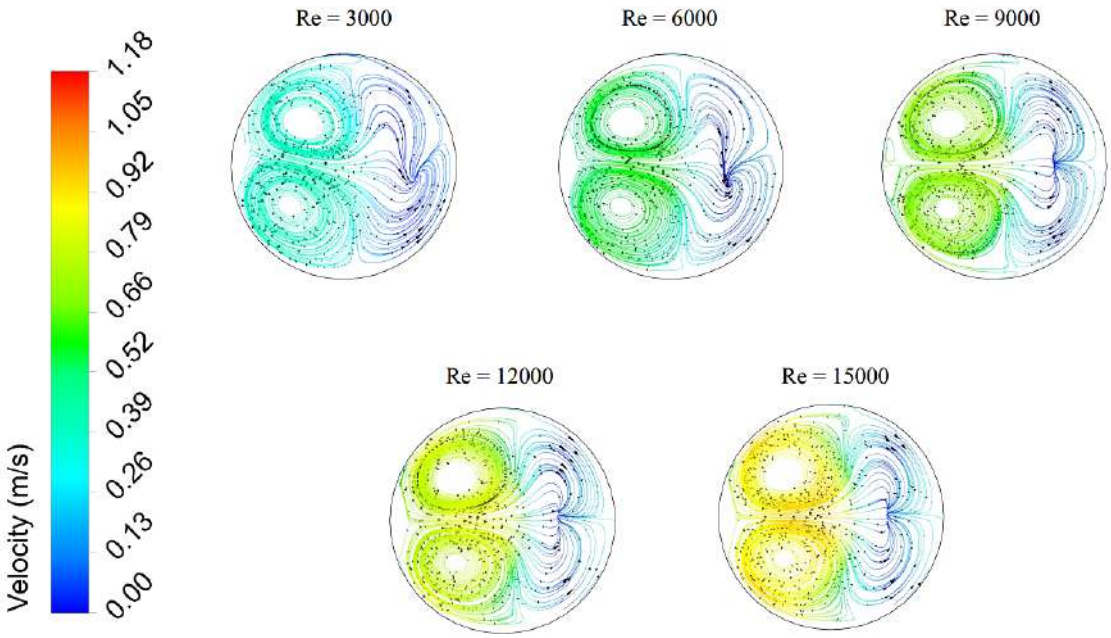

Figure 7. Streamlines at the cross-section of case D.

As can be seen in Fig. 5, 6 and 7, cases B, C and D presented the phenomenon of secondary flow (swirl), which, according to Chang *et al*. (2020) and Bergman *et al*. (2014), is a phenomenon that tends to increase the heat transfer rate, what is consistent with the maximum velocity values calculated for each case. In this case, the secondary flow is manly characterized by the presence of Dean vortices that are generated downstream the curves in the pipes. For the same inlet velocity, case A had the lowest maximum velocity because it does not present secondary flow, case B (helical), despite the swirl effect generated, does not have abrupt change zones in the flow direction (e.g., pipe knees), obtaining the second-lowest maximum velocity, and cases C and D had the highest maximum velocity calculated among all cases, obtained for both in a cross-section located after the first pipe knee and located into the Dean vortices. The difference between the last two cases is precisely due to the number of duct knees along with the coil, which significantly influences the heat transfer rate. Figure 8 presents the variation of the Dean number with the Reynolds number for the cases analyzed.

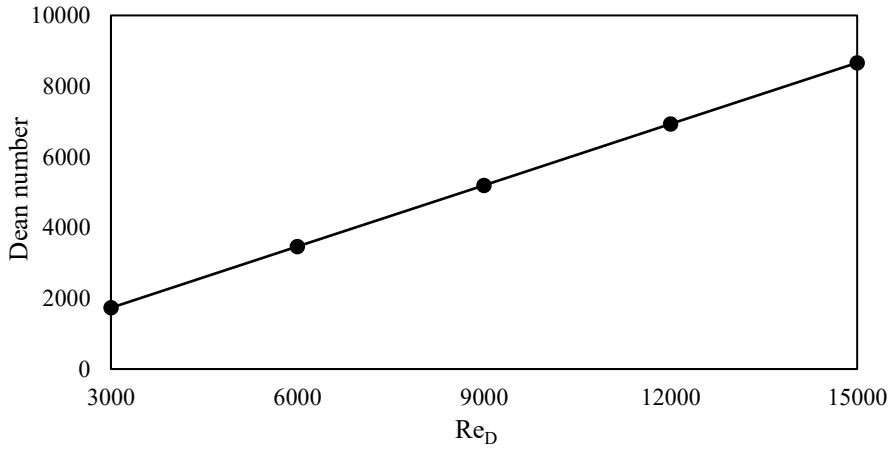

Figure 8. Dean number as a function of Reynolds number, for D = 20 mm and R_c = 30 mm.

As can be seen, the Dean number has a linear behavior with the Reynolds number, what is in accordance with the results showed in Figs. 5- 7, that showed the intensification of the vortices with the increase of the Reynolds number. The maximum velocity registered in cases C and D, with Re = 15000, was 1.18 m/s, which is twice of the value of the inlet velocity (0.58 m/s).

In order to directly visualize the heat transfer potential of each geometry, Fig. 9 presents, for each one of the analyzed cases, the Nusselt number as a function of the Reynolds number, both calculated considering the diameter D as the geometric characteristic.

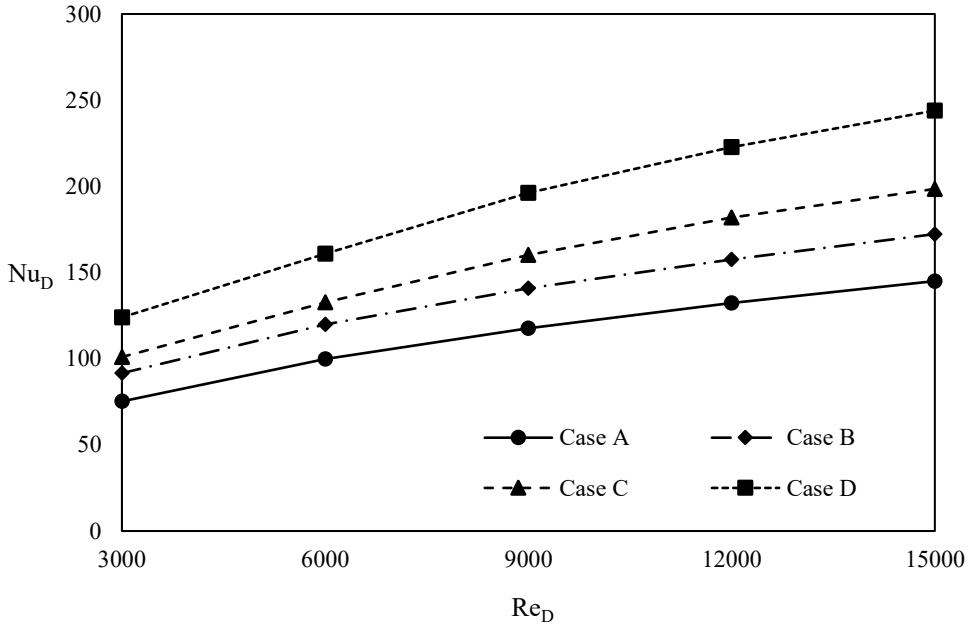

Figure 9. Nusselt number as a function of the Reynolds number for all cases analyzed.

As predicted by the analysis of secondary flow in each coil type, the case with the highest heat transfer capacity was the case D (coil with vertical ducts), followed by cases C, B and A. The pattern observed is that the more disturbed is the flow, with more three-dimensional swirl effects, the higher is the heat transfer rate. However, it is important to consider that the pressure drop in these cases tends to increase. Figure 10 presents the thermal-hydrodynamic performance index curves, for cases B, C and D, as defined in Eq. 10, as a function of the Reynolds number.

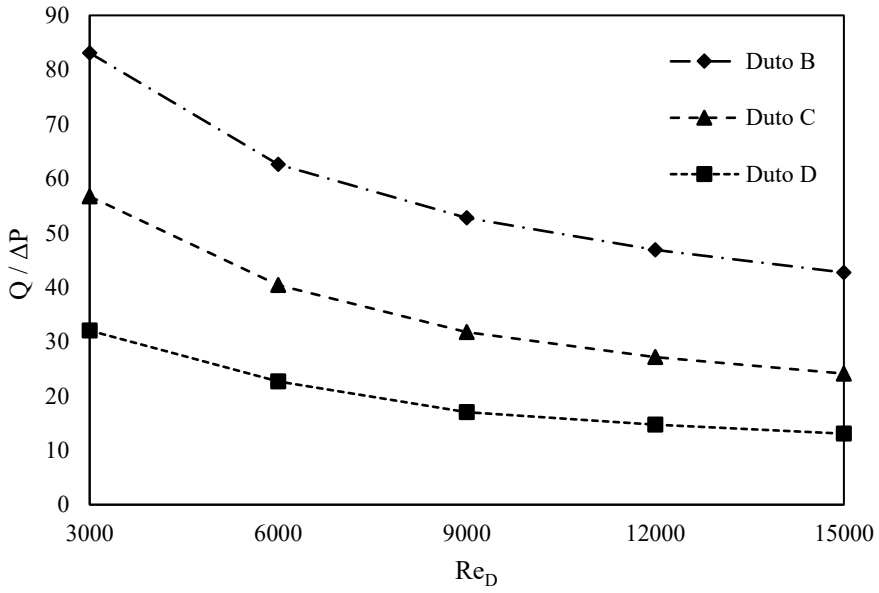

Figure 10. Heat transfer-pressure drop ratio as a function of the Reynolds number for cases B, C and D.

Figure 10 revels that, in addition to the increase of the heat transfer capacity, the pressure drop tends to increase considerably. In this way, despite of guarantee the highest heat transfer rate, the case D has a significant pressure drop due to the large number of pipe knees and, therefore, local losses. According to the Fig. 9, the case that has the best cost-benefit relation is the case B (helicoidal coil), what can be explained by their smooth curve characteristic.

4. CONCLUSIONS

This paper aimed to analyze four different coil geometries for a shell and tube heat exchanger, in order to identify the general aspects of the flow and, mainly, the heat exchange capacity of each one. Based on the results presented in Section 3, obtained through the procedure described in Section 2, can be concluded that:

1. The helical coil, the coil with horizontal ducts and the coil with vertical ducts, i.e., cases B, C and D, induced the formation of secondary flow effects (swirl). This effect tends to improve the heat transfer rate;
2. Among the geometries that generated secondary flow, cases C and D had the highest maximum velocity, obtained in a cross-section located after the first pipe knee of each one;
3. From the analysis of the Nusselt number as a function of the Reynolds number, the geometry with the highest heat exchange capacity is the coil with vertical ducts geometry (case D), which presents more abrupt changes in the flow direction (more knees), and therefore more intense swirl phenomenon;
4. The best cost-benefit, in terms of the thermal-hydrodynamic performance, was reached by the case B (helicoidal coil), due to their geometric characteristic of smooth curves along all the duct, without abrupt changes in the flow direction.

5. ACKNOWLEDGEMENTS

The authors would like to thank the Computational Fluid Dynamics Laboratory of the Federal University of Rio Grande do Norte (UFRN) for the infrastructure available for the development of this research.

6. REFERENCES

Bergman, T. L., Lavine, A. S., Incropera, F. P., and Dewitt. “Fundamentos de transferência de calor e de massa”. 2014. 7ª ed. – Rio de Janeiro. LTC.

Çelik, I. B., Ghia, U., Roache, P. J., Freitas, C. J., Coleman, H. and Raad, P. E., 2008. “Procedure for Estimation and Reporting of Uncertainty Due to Discretization in CFD Applications”. Journal of Fluids Engineering, Vol. 130, No. 7. ISSN 0098-2202. doi:10.1115/1.2960953.

Chang, S. W., Wu, P. -S., Cai, W. L., and Liu, J. H., 2020. “Turbulent flow and heat transfer of helical coils with twisted section”. Applied Thermal Engineering, Vol. 180, No. 115919.

Fouda, A.; Nada, S. A.; Elattar, H. F.; Refaey, H. A.; Bin-Mahfouz, A. S, 2018. “Thermal performance modeling of turbulent flow in multi tube in tube helically coiled heat exchangers”. International Journal of Mechanical Sciences, Vol. 135, p. 621-638. doi: 10.1016/j.ijmecsci.2017.12.015.

Versteeg, H.K. and Malalasekera, W., 2007. An Introduction to Computational Fluid Dynamics: The Finite Volume Method. Pearson Education Limited, Harlow, 2nd edition.

Vivekanandan, M., Venkatesh, R., Periyasamy, R., Mohankumar, S., and Devakumar, L. 2020. “Experimental and CFD investigation of helical coil heat exchanger with flower baffle”. Materials Today: Proceedings.

Wilcox, D. C. 2008. "Formulation of the k-omega Turbulence Model Revisited," AIAA Journal, Vol. 46, No. 11, pp. 2823-2838.

7. RESPONSIBILITY NOTICE

The authors are the only responsible for the printed material included in this paper.